Fast and Accurate Computation of Hypersingular Integrals in Galerkin Surface Integral Equation Formulations via the Direct Evaluation Method

Athanasios G. Polimeridis, José M. Tamayo, Juan M. Rius, *Senior Member, IEEE*, and Juan R. Mosig, *Fellow, IEEE*

Abstract—**Hypersingular 4-D integrals, arising in the Galerkin discretization of surface integral equation formulations, are computed by means of the direct evaluation method. The proposed scheme extends the basic idea of the singularity cancellation methods, usually employed for the regularization of the singular integral kernel, by utilizing a series of coordinate transformations combined with a reordering of the integrations. The overall algebraic manipulation results in smooth 2-D integrals that can be easily evaluated via standard quadrature rules. Finally, the reduction of the dimensionality of the original integrals together with the smooth behavior of the associated integrands lead up to unmatched accuracy and efficiency.**

Index Terms—**Electromagnetic (EM) scattering, method of moments (MoM), numerical analysis, singular integrals, surface integral equations.**

I. INTRODUCTION

SURFACE integral equation formulations are proven to be one of the most powerful methods for the solution of various electromagnetic (EM) antenna and scattering problems [1]–[3]. Galerkin variants of the method of moments (MoM) [4] are most often utilized for the numerical solution of these electromagnetic surface integral equations, calling for the calculation of four-dimensional (or double) integrals with singular kernels. Typically, the singular integrals arising in surface field integral equations can be categorized according to the behavior of the kernel into weakly singular $(1/R)$, strongly singular $(1/R^2)$ and hypersingular $(1/R^3)$. In EM community, though, the definition might be quite different, i.e., kernels with $1/R^2$ and $1/R^3$ behaviors are called hypersingular and super hypersingular, respectively, as discussed in detail by Tong and Chew [5], [6].

To be more specific, weakly singular integrals appear in the electric field integral equation (EFIE) formulations, when divergence-conforming basis and testing functions, like the popular Rao-Wilton-Glisson (RWG) [7], are incorporated in the Galerkin MoM. Due to the non smooth behavior of the weakly singular integral kernels, classical numerical quadrature rules fail to meet the requirements for high precision results, and more sophisticated techniques are needed to tackle this problem. Generally, various regularization methods for the computation of 4-D weakly singular integrals have appeared in the literature over the last decades and interested readers could consult [8] for a more detailed history of relevant previous work.

On the other hand, 4-D hypersingular integrals (following here and for the rest of the manuscript the convention used in EM community) arise in the numerical solution of magnetic field integral equation (MFIE) and combined field integral equation (CFIE) formulations, since the latter are combination of EFIE and MFIE formulations. Over the last years, numerous techniques have been presented for the accurate and efficient evaluation of those multidimensional hypersingular integrals, which can be roughly categorized into two main families: singularity cancellation methods [9]–[13] and singularity subtraction methods [14]–[24]. The logical expectation is that both methods should lead to superior accuracy compared with direct implementation of quadrature rules. This is not necessarily the case, as demonstrated in this paper, especially when the quest for machine precision is combined with the need for improved efficiency.

In this paper, the direct evaluation method tailored for the hypersingular integrals arising in Galerkin surface integral equation formulations is developed. The proposed method utilizes a series of coordinate transformations together with a reordering of the integrations in order to reduce the dimensionality of the 4-D hypersingular integrals into 2-D smooth integrals that can be easily computed via generalized Cartesian product rules based on standard Gauss quadratures, readily available in the literature. The direct evaluation method was originally introduced by Gray *et al.* [25], [26] for the evaluation of super hypersingular Galerkin surface integrals arising in static problems and recently it was extended by the first author for the case of the weakly singular integrals in Galerkin MoM problems over coincident [8] and over edge adjacent and vertex adjacent triangle elements [27].

In Section II, the singular integrals arising in Galerkin surface integral equation formulations are reported. In Section III, the direct evaluation method for the hypersingular integrals over

edge adjacent triangle elements is presented in detail. The final formulas in the last part of Section III together with the functions provided in Appendix A form the complete setup for a convenient software implementation. Finally, in Section IV, the proposed method is applied in a typical test case problem and the results are compared with some of the most powerful methods available in the literature.

II. SINGULAR INTEGRALS

The evaluation of the Galerkin MoM matrix elements in EFIE, MFIE, or CFIE formulations, using RWG basis functions $\mathbf{f}$ and either RWG or $\hat{\mathbf{n}} \times$ RWG testing functions $\mathbf{g}$, calls for the calculation of the following singular integrals [19]:

$$I_1 := \int_{S_m} \mathbf{g}(\mathbf{r}) \cdot \nabla \int_{S_n} G(\mathbf{r}, \mathbf{r}') \nabla_s' \cdot \mathbf{f}(\mathbf{r}') \, dS' dS \quad (1)$$

$$I_2 := \int_{S_m} \mathbf{g}(\mathbf{r}) \cdot \int_{S_n} G(\mathbf{r}, \mathbf{r}') \, \mathbf{f}(\mathbf{r}') \, dS' dS \quad (2)$$

$$I_3 := \int_{S_m} \mathbf{g}(\mathbf{r}) \cdot \int_{S_n} \nabla G(\mathbf{r}, \mathbf{r}') \times \mathbf{f}(\mathbf{r}') \, dS' dS \quad (3)$$

which incorporate the free-space Green's function

$$G(\mathbf{r}, \mathbf{r}') = G(R) = \frac{e^{-jkR}}{R} \quad (4)$$

with $R = |\mathbf{r} - \mathbf{r}'|$ being the distance function and $k = \omega\sqrt{\varepsilon\mu}$ the wavenumber. Here, S_m and S_n correspond to the supports of the associated testing and basis functions.

The integrands of the aforementioned integrals become singular when the integration domains S_m and S_n have common points. Consequently, regular numerical quadrature rules can not converge with a reasonable number of integration points and the need appears for more sophisticated techniques to compute them. The integral I_1 can be transformed, for the basis and testing functions under consideration, to a weakly singular integral [19]. Therefore, both I_1 and I_2 can be included in the cases which were already treated in previous works within the framework of the direct evaluation method [8], [27].

Although the basis and testing functions used herein are defined over triangle pairs, the above integrals can be reduced to integrals over the forming triangles, following a "triangle by triangle" assembly procedure to fill the MoM impedance matrix. Hence, we consider the integrals over the triangles E_P and E_Q instead of the domains S_m and S_n. In this paper, we focus particularly on the solution of the hypersingular integral

$$I := \int_{E_P} \mathbf{g}(\mathbf{r}) \cdot \int_{E_Q} \nabla G(\mathbf{r}, \mathbf{r}') \times \mathbf{f}(\mathbf{r}') \, dS' dS \quad (5)$$

when the triangles E_P and E_Q lie on different planes while sharing a common edge.

III. DIRECT EVALUATION METHOD

A. Equilateral Triangle Parameter Space

The first step of the direct evaluation method is to introduce an appropriate parameter space. In this manuscript, an equilateral parameter space $\{\eta, \xi\}$, where $-1 \leq \eta \leq 1, 0 \leq \xi \leq \sqrt{3}(1 - |\eta|)$ (see Fig. 1) is employed for each one of the triangles, following the original work by Gray *et al.* [25], [26]. This
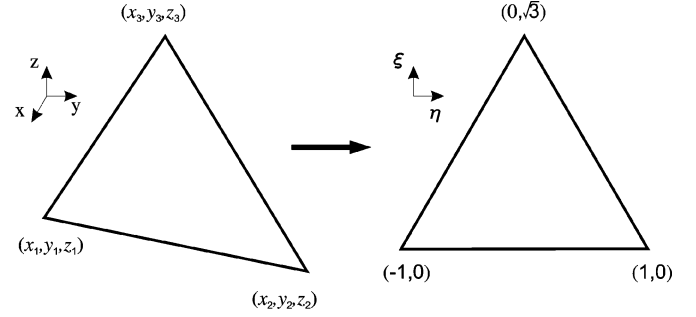

Fig. 1. Equilateral parameter space transformation (original triangle $\rightarrow$ master triangle).

specific choice of parameter space is rather convenient for executing the edge adjacent integration, in which we are interested here, due to its symmetry. The governing transformation matrices are given by

$$\mathbf{r} = \begin{bmatrix} x \\ y \\ z \end{bmatrix} = \begin{bmatrix} \frac{x_2+x_1}{2} \\ \frac{y_2+y_1}{2} \\ \frac{z_2+z_1}{2} \end{bmatrix} + \begin{bmatrix} \frac{x_2-x_1}{2} & \frac{2x_3-x_1-x_2}{2\sqrt{3}} \\ \frac{y_2-y_1}{2} & \frac{2y_3-y_1-y_2}{2\sqrt{3}} \\ \frac{z_2-z_1}{2} & \frac{2z_3-z_1-z_2}{2\sqrt{3}} \end{bmatrix} \begin{bmatrix} \eta \\ \xi \end{bmatrix}$$

$$= [\mathbf{A}] + [\mathbf{Q}] \begin{bmatrix} \eta \\ \xi \end{bmatrix} \quad (6)$$

with the Jacobian being a constant, $J = A/\sqrt{3}$, where A is the area of the original triangle. The hypersingular integral (5) in the new parametric space can be evaluated as

$$I = (J_p J_q) \int_{-1}^{1} d\eta \int_0^{\xi(\eta)} d\xi \int_{-1}^{1} d\eta' \int_0^{\xi(\eta')} \\ \times \mathbf{g}(\eta, \xi) \cdot (\nabla G(R) \times \mathbf{f}(\eta', \xi')) d\xi' \quad (7)$$

where $\xi(\eta) = \sqrt{3}(1 - |\eta|)$ and J_p and J_q are the associated Jacobians of the transformation from the original triangles to the equilateral parameter space master triangles. Moreover, R is a function of all six nodal coordinates (for the two original triangles) as well as the four variables (two for the inner integral E_Q and two for the outer integral E_P) of the equilateral triangle parameter space.

Next, we need to orient the elements so that the shared edge is defined by $\xi = 0$ for E_P, and $\xi' = 0$ for E_Q, hence, the singularity is characterized by $\eta + \eta' = \xi = \xi' = 0$ (see Fig. 2). The position vectors in the new parametric space are given according to (6), taking into account the notation in Fig. 2, where $E_P : (\mathbf{r}_{1p}, \mathbf{r}_{2p}, \mathbf{r}_{3p}) \equiv (\mathbf{r}_1, \mathbf{r}_2, \mathbf{r}_3)$ and $E_Q : (\mathbf{r}_{1q}, \mathbf{r}_{2q}, \mathbf{r}_{3q}) \equiv (\mathbf{r}_2, \mathbf{r}_1, \mathbf{r}_4)$

$$\mathbf{r} = \mathbf{r_P} = [\mathbf{A_P}] + [\mathbf{Q_P}] \begin{bmatrix} \eta \\ \xi \end{bmatrix}$$

$$= \begin{bmatrix} \frac{x_2+x_1}{2} \\ \frac{y_2+y_1}{2} \\ \frac{z_2+z_1}{2} \end{bmatrix} + \begin{bmatrix} \frac{x_2-x_1}{2} & \frac{2x_3-x_1-x_2}{2\sqrt{3}} \\ \frac{y_2-y_1}{2} & \frac{2y_3-y_1-y_2}{2\sqrt{3}} \\ \frac{z_2-z_1}{2} & \frac{2z_3-z_1-z_2}{2\sqrt{3}} \end{bmatrix} \begin{bmatrix} \eta \\ \xi \end{bmatrix} \quad (8)$$

$$\mathbf{r}' = \mathbf{r_Q} = [\mathbf{A_Q}] + [\mathbf{Q_Q}] \begin{bmatrix} \eta' \\ \xi' \end{bmatrix}$$

$$= \begin{bmatrix} \frac{x_2+x_1}{2} \\ \frac{y_2+y_1}{2} \\ \frac{z_2+z_1}{2} \end{bmatrix} + \begin{bmatrix} \frac{x_1-x_2}{2} & \frac{2x_4-x_1-x_2}{2\sqrt{3}} \\ \frac{y_1-y_2}{2} & \frac{2y_4-y_1-y_2}{2\sqrt{3}} \\ \frac{z_1-z_2}{2} & \frac{2z_4-z_1-z_2}{2\sqrt{3}} \end{bmatrix} \begin{bmatrix} \eta' \\ \xi' \end{bmatrix} \quad (9)$$
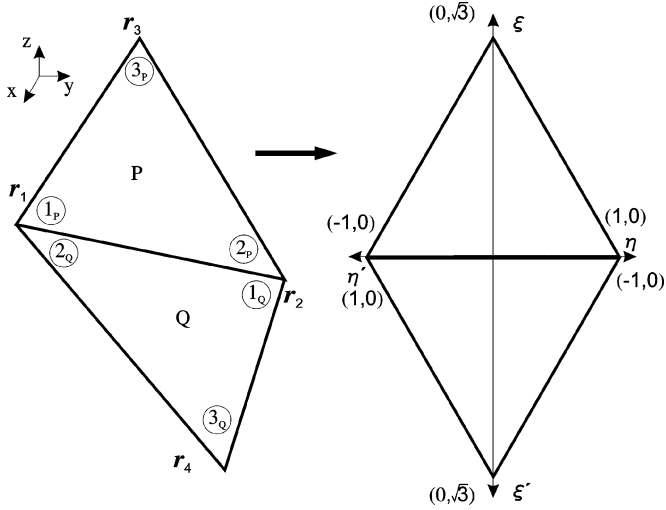
Fig. 2. Orientation of the triangular elements both in the original and the equilateral triangle parameter space.
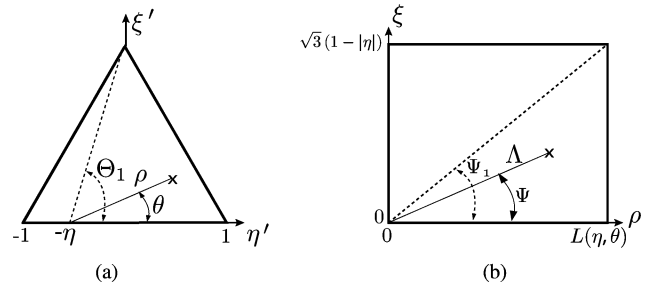

Fig. 3. Polar coordinate transformations employed in the first analytical integration. (a) First transformation: $\{\eta', \xi'\} \rightarrow \{\rho, \theta\}$. (b) Second transformation: $\{\rho, \xi\} \rightarrow \{\Lambda, \Psi\}$.

and the distance function R can be derived as follows:

$$
\begin{aligned}
R &= |\mathbf{r_P} - \mathbf{r_Q}| \\
&= \Big(|\boldsymbol{\alpha}_{e_2}|^2 \xi^2 + 2\xi[(\boldsymbol{\alpha}_{e_2} \cdot \boldsymbol{\alpha}_{e_3})\xi' + (\boldsymbol{\alpha}_{e_1} \cdot \boldsymbol{\alpha}_{e_2})(\eta + \eta')] \\
&\quad + |\boldsymbol{\alpha}_{e_1}|^2(\eta + \eta')^2 + |\boldsymbol{\alpha}_{e_3}|^2 \xi'^2 \\
&\quad + 2(\boldsymbol{\alpha}_{e_1} \cdot \boldsymbol{\alpha}_{e_3})(\eta + \eta')\xi' \Big)^{1/2}
\end{aligned}
\tag{10}
$$

where

$$
\begin{aligned}
\boldsymbol{\alpha}_{e_1} &= \frac{\mathbf{r}_2 - \mathbf{r}_1}{2} \\
\boldsymbol{\alpha}_{e_2} &= \frac{2\mathbf{r}_3 - \mathbf{r}_1 - \mathbf{r}_2}{2\sqrt{3}} \\
\boldsymbol{\alpha}_{e_3} &= -\frac{2\mathbf{r}_4 - \mathbf{r}_1 - \mathbf{r}_2}{2\sqrt{3}}
\end{aligned}
\tag{11}
$$

which only depend on the vertices of the triangles.

B. First Analytical Integration

Thereafter, a polar coordinate transformation within the inner integration (triangle Q) is introduced to cancel the line of singularity defined by $\xi = \xi' = 0$ and $\eta = -\eta'$

$$
\begin{aligned}
\eta' &= \rho \cos(\theta) - \eta \\
\xi' &= \rho \sin(\theta).
\end{aligned}
\tag{12}
$$

The distance function takes the form

$$
R = \sqrt{\beta_{e_1} \xi^2 + \beta_{e_2} \xi \rho + \beta_{e_3} \rho^2}
\tag{13}
$$

where

$$
\begin{aligned}
\beta_{e_1} &= |\boldsymbol{\alpha}_{e_2}|^2 \\
\beta_{e_2} &= 2[(\boldsymbol{\alpha}_{e_1} \cdot \boldsymbol{\alpha}_{e_2})\cos(\theta) + (\boldsymbol{\alpha}_{e_2} \cdot \boldsymbol{\alpha}_{e_3})\sin(\theta)]
\end{aligned}
$$

$$
\begin{aligned}
\beta_{e_3} &= |\boldsymbol{\alpha}_{e_1}|^2 \cos^2(\theta) + 2(\boldsymbol{\alpha}_{e_1} \cdot \boldsymbol{\alpha}_{e_3}) \cos(\theta) \sin(\theta) \\
&\quad + |\boldsymbol{\alpha}_{e_3}|^2 \sin^2(\theta).
\end{aligned}
\tag{14}
$$

The integration with respect to θ should be split into two pieces, as shown in Fig. 3(a)

$$
\begin{aligned}
I = \frac{A_p A_q}{3} \int_{-1}^{1} d\eta \int_{0}^{\xi(\eta)} d\xi \\
\times \Bigg[\int_{0}^{\Theta_1(\eta)} d\theta \int_{0}^{L(\eta,\theta)} \mathbf{g}(\eta,\xi) \cdot (\nabla G \times \mathbf{f}(\eta,\theta,\rho))\rho d\rho \\
+ \int_{\Theta_1(\eta)}^{\pi} d\theta \int_{0}^{L(\eta,\theta)} \mathbf{g}(\eta,\xi) \cdot (\nabla G \times \mathbf{f}(\eta,\theta,\rho))\rho d\rho \Bigg]
\end{aligned}
\tag{15}
$$

where

$$
\Theta_1(\eta) = \frac{\pi}{2} - \tan^{-1}\left(\frac{\eta}{\sqrt{3}}\right)
$$

$$
L(\eta,\theta) = \begin{cases} \frac{\sqrt{3}(1+\eta)}{\sin(\theta)+\sqrt{3}\cos(\theta)}, & 0 < \theta < \Theta_1 \\ \frac{\sqrt{3}(1-\eta)}{\sin(\theta)-\sqrt{3}\cos(\theta)}, & \Theta_1 < \theta < \pi. \end{cases}
\tag{16}
$$

Bearing in mind that the breakpoint in θ is only a function of η, the integration can be directly rearranged

$$
\begin{aligned}
I = \frac{A_p A_q}{3} \int_{-1}^{1} d\eta \int_{0}^{\Theta_1(\eta)} d\theta \int_{0}^{\xi(\eta)} d\xi \int_{0}^{L(\eta,\theta)} \\
\times \mathbf{g}(\eta,\xi) \cdot (\nabla G(R) \times \mathbf{f}(\eta,\theta,\rho))\rho d\rho \\
+ \frac{A_p A_q}{3} \int_{-1}^{1} d\eta \int_{\Theta_1(\eta)}^{\pi} d\theta \int_{0}^{\xi(\eta)} d\xi \int_{0}^{L(\eta,\theta)} \\
\times \mathbf{g}(\eta,\xi) \cdot (\nabla G(R) \times \mathbf{f}(\eta,\theta,\rho))\rho d\rho.
\end{aligned}
\tag{17}
$$

As the singularity now occurs when $\rho = \xi = 0$, we proceed in accordance with [25] by introducing a second polar coordinate transformation

$$
\begin{aligned}
\rho &= \Lambda \cos(\Psi) \\
\xi &= \Lambda \sin(\Psi)
\end{aligned}
\tag{18}
$$

as shown in Fig. 3(b). The distance function in the new parametric system takes the form

$$R = \Lambda \sqrt{\beta_{e_1} \sin^2(\Psi) + \beta_{e_2} \sin(\Psi)\cos(\Psi) + \beta_{e_3}\cos^2(\Psi)}$$
$$= \Lambda B(\theta, \Psi) \quad (19)$$

and the original integral can be written as a sum of 3-D integrals

$$I = \sum_{l=0}^{1} \sum_{m=0}^{1} \int_{-1}^{1} d\eta \int_{\Theta_l}^{\Theta_{l+1}} d\theta \int_{\Psi_m}^{\Psi_{m+1}} A(\eta, \theta, \Psi) d\Psi \quad (20)$$

since the integral over Λ

$$A(\eta, \theta, \Psi) = \frac{A_p A_q}{3} \cos(\Psi) \int_0^{\Lambda_L} \mathbf{g}(\eta, \Lambda, \Psi)$$
$$\cdot (\nabla G(R) \times \mathbf{f}(\eta, \theta, \Lambda, \Psi)) \Lambda^2 d\Lambda \quad (21)$$

can be evaluated analytically, as will be shown later. In the last expression, one can easily identify the final Jacobian after the whole set of parametric transformations

$$J = \frac{A_p A_q}{3} \Lambda^2 \cos(\Psi). \quad (22)$$

The main kernel of the hypersingular integral can be extended as

$$\nabla G(R) = \nabla \left(\frac{e^{-jkR}}{R} \right) = -\frac{e^{-jkR}}{R^3} (1 + jkR)\mathbf{R} \quad (23)$$

where also the distance vector $\mathbf{R} = \mathbf{r_P} - \mathbf{r_Q}$ is proportional to Λ

$$\mathbf{R} = \Lambda \mathbf{B}(\theta, \Psi)$$
$$\mathbf{B} = \boldsymbol{\alpha}_{e_2} \sin(\Psi) + \boldsymbol{\alpha}_{e_1} \cos(\Psi)\cos(\theta)$$
$$+ \boldsymbol{\alpha}_{e_3} \cos(\Psi)\sin(\theta). \quad (24)$$

Substituting (19) and (24) in (23) yields

$$\nabla G(R) = -\frac{e^{-jk\Lambda B(\theta, \Psi)}}{\Lambda^2 B(\theta, \Psi)^3} (1 + jk\Lambda B(\theta, \Psi))\mathbf{B}(\theta, \Psi). \quad (25)$$

One of the key points of the direct evaluation method is that the singularity $1/\Lambda^2$ is canceled out with the Jacobian (22), obtaining finally

$$A(\eta, \theta, \Psi) = \frac{A_p A_q}{3} \frac{\cos(\Psi)}{B(\theta, \Psi)^3} \int_0^{\Lambda_L} e^{-jk\Lambda B(\theta, \Psi)}$$
$$\times (1 + jk\Lambda B(\theta, \Psi))\mathbf{g}(\eta, \Lambda, \Psi) \cdot (\mathbf{f}(\eta, \theta, \Lambda, \Psi)$$
$$\times \mathbf{B}(\theta, \Psi)) d\Lambda. \quad (26)$$

Inasmuch as the testing and basis functions $\mathbf{g}(\eta, \Lambda, \Psi)$ and $\mathbf{f}(\eta, \theta, \Lambda, \Psi)$ are either RWG or $\hat{\mathbf{n}} \times$ RWG functions, it is easy to prove that after applying the parametric transformations they have the following pattern:

$$\mathbf{v}_1(\theta, \Psi) + \mathbf{v}_2(\theta, \Psi)\Lambda + \mathbf{v}_3(\theta, \Psi)\eta \quad (27)$$

where $\mathbf{v}_1$, $\mathbf{v}_2$ and $\mathbf{v}_3$ are vectors independent of Λ and η, and are determined by the actual functions we use. Consequently, in (26), only terms proportional (considering the variable Λ) to any of the following:

TABLE I
FUNCTIONS $M_i(\eta, \Lambda, B)$

$M_1(\eta, \Lambda, B) = 1$	$M_7(\eta, \Lambda, B) = \eta^2$
$M_2(\eta, \Lambda, B) = e^{-jkB\Lambda}$	$M_8(\eta, \Lambda, B) = \eta e^{-jkB\Lambda}$
$M_3(\eta, \Lambda, B) = \Lambda e^{-jkB\Lambda}$	$M_9(\eta, \Lambda, B) = \eta^2 e^{-jkB\Lambda}$
$M_4(\eta, \Lambda, B) = \Lambda^2 e^{-jkB\Lambda}$	$M_{10}(\eta, \Lambda, B) = \eta\Lambda e^{-jkB\Lambda}$
$M_5(\eta, \Lambda, B) = \Lambda^3 e^{-jkB\Lambda}$	$M_{11}(\eta, \Lambda, B) = \eta^2\Lambda e^{-jkB\Lambda}$
$M_6(\eta, \Lambda, B) = \eta$	$M_{12}(\eta, \Lambda, B) = \eta\Lambda^2 e^{-jkB\Lambda}$

$$e^{-jk\Lambda B(\theta, \Psi)}; \quad \Lambda e^{-jk\Lambda B(\theta, \Psi)}$$
$$\Lambda^2 e^{-jk\Lambda B(\theta, \Psi)}; \quad \Lambda^3 e^{-jk\Lambda B(\theta, \Psi)} \quad (28)$$

appear. Of course, all of them can be analytically integrated with respect to Λ, therefore, justifying the argument below (21).

After the first analytical integration, which can be held with the help of a symbolic mathematical software like *Maple* for the sake of a systematic approach, the function A takes the form

$$A(\eta, \theta, \Psi) = \sum_{i=1}^{12} c_i(\theta, \Psi) M_i(\eta, \Lambda_L(\eta, \theta, \Psi), B(\theta, \Psi)) \quad (29)$$

where $M_i(\eta, \Lambda, B)$ are fixed functions defined in Table I and the coefficients $c_i(\theta, \Psi)$ depend on the actual functions $\mathbf{g}$ and $\mathbf{f}$ under consideration.

The integration limits in (20) are given by

$$\Theta_0 = 0; \quad \Theta_1 = \frac{\pi}{2} - \tan^{-1}\left(\frac{\eta}{\sqrt{3}}\right); \quad \Theta_2 = \pi \quad (30)$$

and

$$\Psi_0 = 0; \quad \Psi_1 = \tan^{-1}\left(\frac{\sqrt{3}(1 - |\eta|)}{L(\eta, \theta)}\right); \quad \Psi_2 = \frac{\pi}{2} \quad (31)$$

while the integration limits with respect to Λ take the following form:

$$\Lambda_L(\eta, \theta, \Psi) = \begin{cases} \frac{L(\eta, \theta)}{\cos(\Psi)}, & \Psi_0 < \Psi < \Psi_1 \\ \frac{\sqrt{3}(1 - |\eta|)}{\sin(\Psi)}, & \Psi_1 < \Psi < \Psi_2. \end{cases} \quad (32)$$

Since the angle integrals cannot be evaluated analytically, it will be necessary to rearrange the aforementioned integrals by placing the η integral in the innermost position, taking into account that the functions $M_i(\eta, \Lambda, B)$ can be integrated analytically in terms of η. As a last remark, note that for some combinations of testing and basis functions $\mathbf{g}$ and $\mathbf{f}$, only some of the terms in (29) appear, reducing the actual computational cost for those cases.

C. Second Analytical Integration

In the next step, the integration is split for positive and negative values of η. Exploiting the symmetry of the equilateral tri-

angle parameter space, though, it suffices to proceed only to the analytical integration over region $\eta \geq 0$ [26]. The remaining part can be easily computed by flipping the elements around, as presented in part D of this section.

Before starting with the second analytical integration, we introduce the three possible values of the function Λ_L, for the case $\eta \geq 0$, depending on the zone of the $\{\theta, \Psi\}$ plane

$$
\begin{aligned}
\Lambda_{L_1} &= \frac{\sqrt{3}(1-\eta)}{\cos(\Psi)(\sin(\theta) - \sqrt{3}\cos(\theta))} \\
\Lambda_{L_2} &= \frac{\xi(\eta)}{\sin(\Psi)} = \frac{\sqrt{3}(1-\eta)}{\sin(\Psi)} \\
\Lambda_{L_3} &= \frac{\sqrt{3}(1+\eta)}{\cos(\Psi)(\sin(\theta) + \sqrt{3}\cos(\theta))}.
\end{aligned}
\tag{33}
$$

1) Integration Over Region $\Theta_1 \leq \theta \leq \pi$: In this case, the splitting of Ψ integrals is independent of η, thus, leading, without complication, to the following two integrals:

$$
\begin{aligned}
I^{\theta+} &= \int_0^1 d\eta \int_{\theta_\eta}^\pi d\theta \int_0^{\Psi_1^+} A(\eta, \theta, \Psi) d\Psi \\
&+ \int_0^1 d\eta \int_{\theta_\eta}^\pi d\theta \int_{\Psi_1^+}^{\pi/2} A(\eta, \theta, \Psi) d\Psi
\end{aligned}
\tag{34}
$$

where the upper limit of the integration with respect to Λ (manifested as a parameter in the M functions) is different in the two terms

$$
\Lambda_L = \begin{cases} \Lambda_{L_1}, & 0 < \Psi < \Psi_1 \\ \Lambda_{L_2}, & \Psi_1 < \Psi < \frac{\pi}{2}. \end{cases}
\tag{35}
$$

Moreover

$$
\theta_\eta \equiv \Theta_1 = \frac{\pi}{2} - \tan^{-1}\left(\frac{\eta}{\sqrt{3}}\right)
\tag{36}
$$

and the Ψ integral is split at

$$
\Psi_A \triangleq \Psi_1^+ = \tan^{-1}(\sin(\theta) - \sqrt{3}\cos(\theta)).
\tag{37}
$$

Since Ψ_1 is not a function of η, the integral with respect to η can be moved in the innermost integration, once it is interchanged with the θ integral according to the geometry shown in Fig. 4 and the inversion formula

$$
\eta_\theta = \frac{\sqrt{3}}{\tan(\theta)}.
\tag{38}
$$

Finally, switching the integrals results in

$$
\begin{aligned}
I^{\theta+} &= \int_{\pi/2}^\pi d\theta \int_0^{\Psi_A} X^a(\theta, \Psi) d\Psi \\
&+ \int_{\pi/3}^{\pi/2} d\theta \int_0^{\Psi_A} X^b(\theta, \Psi) d\Psi \\
&+ \int_{\pi/2}^\pi d\theta \int_{\Psi_A}^{\pi/2} X^c(\theta, \Psi) d\Psi \\
&+ \int_{\pi/3}^{\pi/2} d\theta \int_{\Psi_A}^{\pi/2} X^d(\theta, \Psi) d\Psi
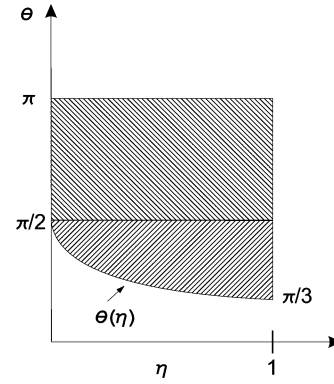\end{aligned}
\tag{39}
$$

Fig. 4. The $\{\eta, \theta\}$ domain for the first shift of the integral, $\Theta_1 \leq \theta \leq \pi$.

where $X^\alpha(\theta, \Psi)$, $\alpha = a, b, c, d$, are the following analytically integrated with respect to η functions:

$$
\begin{aligned}
X^a(\theta, \Psi) &= \int_0^1 A(\Lambda_L = \Lambda_{L_1}) d\eta \\
X^b(\theta, \Psi) &= \int_{\eta_\theta}^1 A(\Lambda_L = \Lambda_{L_1}) d\eta \\
X^c(\theta, \Psi) &= \int_0^1 A(\Lambda_L = \Lambda_{L_2}) d\eta \\
X^d(\theta, \Psi) &= \int_{\eta_\theta}^1 A(\Lambda_L = \Lambda_{L_2}) d\eta.
\end{aligned}
\tag{40}
$$

2) Integration Over Region $0 < \theta \leq \Theta_1$: In this case, the two starting integrals are given by

$$
\begin{aligned}
I^{\theta-} &= \int_0^1 d\eta \int_0^{\theta_\eta} d\theta \int_0^{\Psi_1^-} A(\eta, \theta, \Psi) d\Psi \\
&+ \int_0^1 d\eta \int_0^{\theta_\eta} d\theta \int_{\Psi_1^-}^{\pi/2} A(\eta, \theta, \Psi) d\Psi
\end{aligned}
\tag{41}
$$

where, again

$$
\Lambda_L = \begin{cases} \Lambda_{L_3}, & 0 < \Psi < \Psi_1 \\ \Lambda_{L_2}, & \Psi_1 < \Psi < \frac{\pi}{2} \end{cases}
\tag{42}
$$

and

$$
\theta_\eta \equiv \Theta_1 = \frac{\pi}{2} - \tan^{-1}\left(\frac{\eta}{\sqrt{3}}\right)
\tag{43}
$$

only now the breakpoint in Ψ is a function of η

$$
\begin{aligned}
\Psi_1^- &= \tan^{-1}\left(\frac{\xi(\eta)}{L(\eta, \theta)}\right) \\
&= \tan^{-1}\left(\frac{1-\eta}{1+\eta}[\sin(\theta) + \sqrt{3}\cos(\theta)]\right).
\end{aligned}
\tag{44}
$$

As before, the θ and η integrals are easily interchanged, the domain being the region below the $\theta(\eta)$ curve in Fig. 4. This results in the four integrals

$$
\begin{aligned}
I^{\theta-} &= \int_0^{\pi/3} d\theta \int_0^1 d\eta \int_0^{\Psi_1^-} A(\eta, \theta, \Psi) d\Psi \\
&+ \int_{\pi/3}^{\pi/2} d\theta \int_0^{\eta_\theta} d\eta \int_0^{\Psi_1^-} A(\eta, \theta, \Psi) d\Psi
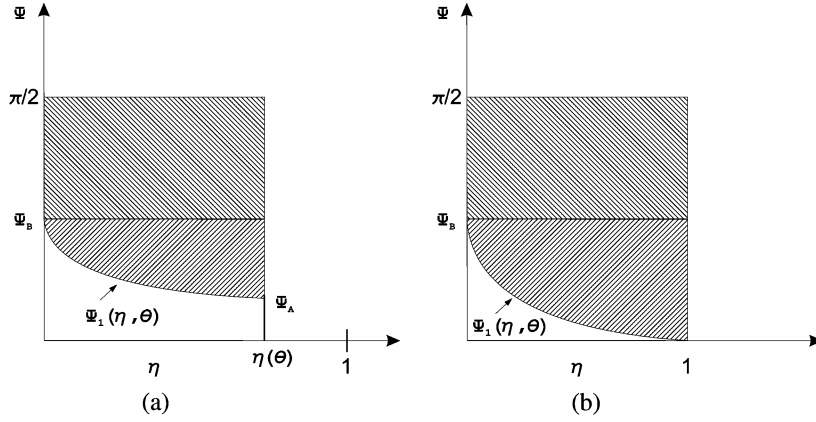\end{aligned}
$$

Fig. 5. The domain for interchanging the integrals $\{\eta, \Psi\}$, for a fixed value of θ. (a) Case $\eta(\theta) < 1$. (b) Case $\eta(\theta) = 1$.

$$+ \int_0^{\pi/3} d\theta \int_0^1 d\eta \int_{\Psi_1^-}^{\pi/2} A(\eta, \theta, \Psi) d\Psi$$

$$+ \int_{\pi/3}^{\pi/2} d\theta \int_0^{\eta_\theta} d\eta \int_{\Psi_1^-}^{\pi/2} A(\eta, \theta, \Psi) d\Psi \quad (45)$$

where η_θ is given in (38). Using the fact that $\Psi_1^-(\eta = 1, \theta) = 0$, the geometry for interchanging η and Ψ is shown in Fig. 5(a) and (b).

3) Integration Over Region $0 < \Psi \leq \Psi_1^-$: Moving the η integral to the front in the first two integrals in (45) $\left(0 < \Psi < \Psi_1^-\right)$ and using that $\Psi_1^-(\eta = \eta_\theta) \equiv \Psi_A$, results in

$$I^{\theta-,\Psi-} = \int_0^{\pi/3} d\theta \int_0^{\Psi_B} X^e(\theta, \Psi) d\Psi$$
$$+ \int_{\pi/3}^{\pi/2} d\theta \int_0^{\Psi_A} X^f(\theta, \Psi) d\Psi$$
$$+ \int_{\pi/3}^{\pi/2} d\theta \int_{\Psi_A}^{\Psi_B} X^g(\theta, \Psi) d\Psi \quad (46)$$

where

$$\Psi_B \triangleq \Psi_1^-(\eta = 0) = \tan^{-1}\left(\sin(\theta) + \sqrt{3}\cos(\theta)\right) \quad (47)$$

and

$$X^e(\theta, \Psi) = X^g(\theta, \Psi) = \int_0^{\Psi_\eta} A(\Lambda_L = \Lambda_{L_3}) d\eta$$
$$X^f(\theta, \Psi) = \int_0^{\eta_\theta} A(\Lambda_L = \Lambda_{L_3}) d\eta. \quad (48)$$

Again, the functions $X^\alpha(\theta, \Psi), \alpha = e, f, g$, are integrated analytically and the integration limit Ψ_η is given by

$$\Psi_\eta = \frac{1 - \frac{\tan(\Psi)}{\sin(\theta) + \sqrt{3}\cos(\theta)}}{1 + \frac{\tan(\Psi)}{\sin(\theta) + \sqrt{3}\cos(\theta)}} = \frac{1 - \gamma}{1 + \gamma}. \quad (49)$$

4) Integration Over Region $\Psi_1^- < \Psi \leq \pi/2$: Similarly, the second two integrals in (45) $\left(\Psi_1^- < \Psi < \pi/2\right)$ become, after the analytical integration with respect to η

$$I^{\theta-,\Psi+} = \int_0^{\pi/3} d\theta \int_0^{\Psi_B} X^h(\theta, \Psi) d\Psi$$

$$+ \int_0^{\pi/3} d\theta \int_{\Psi_B}^{\pi/2} X^i(\theta, \Psi) d\Psi$$

$$+ \int_{\pi/3}^{\pi/2} d\theta \int_{\Psi_A}^{\Psi_B} X^k(\theta, \Psi) d\Psi$$

$$+ \int_{\pi/3}^{\pi/2} d\theta \int_{\Psi_B}^{\pi/2} X^l(\theta, \Psi) d\Psi \quad (50)$$

where

$$X^h(\theta, \Psi) = \int_{\Psi_\eta}^1 A(\Lambda_L = \Lambda_{L_2}) d\eta$$

$$X^i(\theta, \Psi) = \int_0^1 A(\Lambda_L = \Lambda_{L_2}) d\eta$$

$$X^k(\theta, \Psi) = \int_{\Psi_\eta}^{\eta_\theta} A(\Lambda_L = \Lambda_{L_2}) d\eta$$

$$X^l(\theta, \Psi) = \int_0^{\eta_\theta} A(\Lambda_L = \Lambda_{L_2}) d\eta. \quad (51)$$

Finally, by adding all the components from (39), (46), and (50), we end up to the following formula for the integration over positive values of η:

$$I^{\eta+} = I^{\theta-} + I^{\theta+} = I^{\theta-,\Psi-} + I^{\theta-,\Psi+} + I^{\theta+}. \quad (52)$$

More specifically, the hypersingular integral for $\eta > 0$ has been reduced, after regrouping the integrals over disjoint domains in the space $\{\theta, \Psi\}$ (see Fig. 6), to the following 2-D smooth integral:

$$I^{\eta+} = \int_0^{\pi/3} d\theta \int_0^{\Psi_B} \chi^{a+}(\theta, \Psi) d\Psi$$

$$+ \int_{\pi/3}^{\pi/2} d\theta \int_{\Psi_A}^{\Psi_B} \chi^{a+}(\theta, \Psi) d\Psi$$

$$+ \int_{\pi/3}^{\pi/2} d\theta \int_0^{\Psi_A} \chi^{b+}(\theta, \Psi) d\Psi$$

$$+ \int_{\pi/2}^{\pi} d\theta \int_0^{\Psi_A} \chi^{c+}(\theta, \Psi) d\Psi$$

$$+ \int_0^{\pi/2} d\theta \int_{\Psi_B}^{\pi/2} \chi^{d+}(\theta, \Psi) d\Psi$$

$$+ \int_{\pi/2}^{\pi} d\theta \int_{\Psi_A}^{\pi/2} \chi^{d+}(\theta, \Psi) d\Psi \qquad (53)$$

which depends only on the four different functions

$$\chi^{a+}(\theta, \Psi) = X^e + X^h = X^d + X^g + X^k$$
$$= \int_0^{\Psi_\eta} A(\Lambda_L = \Lambda_{L_3}) d\eta$$
$$+ \int_{\Psi_\eta}^1 A(\Lambda_L = \Lambda_{L_2}) d\eta$$

$$\chi^{b+}(\theta, \Psi) = X^b + X^f$$
$$= \int_0^{\eta_\theta} A(\Lambda_L = \Lambda_{L_3}) d\eta$$
$$+ \int_{\eta_\theta}^1 A(\Lambda_L = \Lambda_{L_1}) d\eta$$

$$\chi^{c+}(\theta, \Psi) = X^a = \int_0^1 A(\Lambda_L = \Lambda_{L_1}) d\eta$$

$$\chi^{d+}(\theta, \Psi) = X^i = X^d + X^l = X^c$$
$$= \int_0^1 A(\Lambda_L = \Lambda_{L_2}) d\eta. \qquad (54)$$

The function $\chi^{a+}(\theta, \Psi)$ is defined over the integration domains Ω_1 and Ω_2, $\chi^{b+}(\theta, \Psi)$ over Ω_3, $\chi^{c+}(\theta, \Psi)$ over Ω_4 and $\chi^{d+}(\theta, \Psi)$ over Ω_5 and Ω_6, as shown in Fig. 6. Considering the expressions of A in (29) and the linearity of the integrals, the abovementioned functions equal

$$\chi^{\alpha+}(\theta, \Psi) = \sum_{i=1}^{12} c_i(\theta, \Psi) N_i^\alpha(B(\theta, \Psi), \theta, \Psi) \qquad (55)$$

where $\alpha \in \{a, b, c, d\}$ and the new functions $N_i^\alpha(B, \theta, \Psi)$ are defined using $M_i(\eta, \Lambda, B)$ as

$$N_i^a(B, \theta, \Psi) = \int_0^{\Psi_\eta} M_i(\eta, \Lambda_{L_3}(\eta, \theta, \Psi), B) d\eta$$
$$+ \int_{\Psi_\eta}^1 M_i(\eta, \Lambda_{L_2}(\eta, \theta, \Psi), B) d\eta$$

$$N_i^b(B, \theta, \Psi) = \int_0^{\eta_\theta} M_i(\eta, \Lambda_{L_3}(\eta, \theta, \Psi), B) d\eta$$
$$+ \int_{\eta_\theta}^1 M_i(\eta, \Lambda_{L_1}(\eta, \theta, \Psi), B) d\eta$$

$$N_i^c(B, \theta, \Psi) = \int_0^1 M_i(\eta, \Lambda_{L_1}(\eta, \theta, \Psi), B) d\eta$$

$$N_i^d(B, \theta, \Psi) = \int_0^1 M_i(\eta, \Lambda_{L_2}(\eta, \theta, \Psi), B) d\eta. \qquad (56)$$

D. Equilateral Triangle Parameter Space's Symmetry Effects

The remaining case (integration over negative values of η) can be handled by simply flipping the master triangles (triangles in the equilateral triangle parametric space) and employing the formulas for the $\eta > 0$ case. More specifically, the flipping transformation is stated as
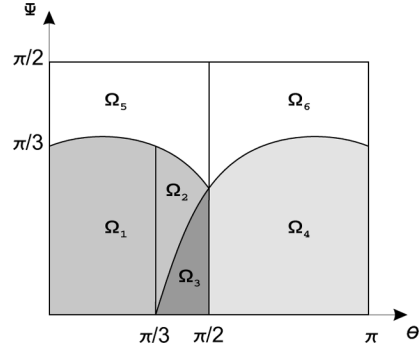

Fig. 6. Integration domains in the $\{\theta, \Psi\}$ space.

$$\begin{bmatrix} \eta \\ \xi \end{bmatrix} = \begin{bmatrix} -1 & 0 \\ 0 & 1 \end{bmatrix} \begin{bmatrix} H \\ \Xi \end{bmatrix} \qquad (57)$$

$$\begin{bmatrix} \eta' \\ \xi' \end{bmatrix} = \begin{bmatrix} -1 & 0 \\ 0 & 1 \end{bmatrix} \begin{bmatrix} H' \\ \Xi' \end{bmatrix} \qquad (58)$$

with the overall additional multiplicative Jacobian being equal to 1. After applying the two polar coordinate transformations, analogously to (12) and (18) but with the extra aforementioned transformation, the distance function R takes the form

$$R = \Lambda B(\pi - \theta, \Psi). \qquad (59)$$

E. Final Formulas

Summarizing, the objective hypersingular integral (5) can be computed by simply evaluating numerically the 2-D smooth integral

$$I = \int_0^{\pi/3} d\theta \int_0^{\Psi_B} \chi^a(\theta, \Psi) d\Psi$$
$$+ \int_{\pi/3}^{\pi/2} d\theta \int_{\Psi_A}^{\Psi_B} \chi^a(\theta, \Psi) d\Psi$$
$$+ \int_{\pi/3}^{\pi/2} d\theta \int_0^{\Psi_A} \chi^b(\theta, \Psi) d\Psi$$
$$+ \int_{\pi/2}^{\pi} d\theta \int_0^{\Psi_A} \chi^c(\theta, \Psi) d\Psi$$
$$+ \int_0^{\pi/2} d\theta \int_{\Psi_B}^{\pi/2} \chi^d(\theta, \Psi) d\Psi$$
$$+ \int_{\pi/2}^{\pi} d\theta \int_{\Psi_A}^{\pi/2} \chi^d(\theta, \Psi) d\Psi \qquad (60)$$

where the functions $\chi^\alpha(\theta, \Psi)$ with $\alpha \in \{a, b, c, d\}$ are given by

$$\chi^\alpha(\theta, \Psi) = \sum_{i=1}^{12} c_i^{\eta^+}(\theta, \Psi) N_i^\alpha(B^+, \theta, \Psi)$$
$$+ c_i^{\eta^-}(\theta, \Psi) N_i^\alpha(B^-, \theta, \Psi) \qquad (61)$$

with

$$B^+ = \sqrt{\beta_{e_1} \sin^2(\Psi) + \beta_{e_2} \sin(\Psi)\cos(\Psi) + \beta_{e_3}\cos^2(\Psi)}$$

$$B^-(\theta,\Psi) = B^+(\pi-\theta,\Psi)$$

$$c_i^{\eta^-}(\theta,\Psi) = c_i^{\eta^+}(\pi-\theta,\Psi)S_i \qquad (62)$$

and the case-dependent sign S_i

$$S_i = \begin{cases} -1, & i = 6, 8, 10, 12 \\ +1, & \text{otherwise.} \end{cases} \qquad (63)$$

Also, $c_i^{\eta^+}(\theta,\Psi)$ are the coefficients of the functions $M_i(\eta, \Lambda_L, B^+)$ in (29) after the first analytical integration and the functions $N_i^\alpha(B,\theta,\Psi)$ are explicitly derived in Appendix A.

IV. NUMERICAL RESULTS

In this section, we present some numerical results for the assessment of the proposed method in terms of accuracy and efficiency. More specifically, it would be sufficient to analyze a single, albeit representative, case among the various combinations of basis and testing functions where all the terms in (28) are present before the first analytical integration. The other possible combinations do not have any particularity which could change the behavior of the results.

To start with, following the notation in Fig. 2, we consider two edge adjacent triangles (T1: $\{\mathbf{r}_1, \mathbf{r}_2, \mathbf{r}_3\}$ and T2: $\{\mathbf{r}_1, \mathbf{r}_2, \mathbf{r}_4\}$) with the following vertices:

$$\mathbf{r}_1 = [0,0,0]; \quad \mathbf{r}_2 = [0,0.1\lambda,0]$$
$$\mathbf{r}_3 = [0,0,0.1\lambda]; \quad \mathbf{r}_4 = [0.1\lambda,0,0] \qquad (64)$$

where $\lambda = 1$ [m] corresponds to the wavelength. Note that $\mathbf{r}_1$ and $\mathbf{r}_2$ are the two common vertices. The actual computed integral is

$$I = \int_{E_P} \mathbf{f}_3(\mathbf{r}) \cdot \int_{E_Q} \nabla G(\mathbf{r},\mathbf{r}') \times \mathbf{f}_1'(\mathbf{r}') \, dS'dS \qquad (65)$$

where $\mathbf{f}_3$ and $\mathbf{f}_1'$ are the RWG functions

$$\mathbf{f}_3(\mathbf{r}) = \frac{|\mathbf{r}_2 - \mathbf{r}_1|}{2A_p}(\mathbf{r} - \mathbf{r}_3)$$

$$\mathbf{f}_1'(\mathbf{r}') = \frac{|\mathbf{r}_4 - \mathbf{r}_2|}{2A_q}(\mathbf{r}' - \mathbf{r}_2). \qquad (66)$$

In Fig. 7(a) and (b), the relative error

$$\varepsilon = \frac{|I - I_{\text{ref}}|}{|I_{\text{ref}}|} \qquad (67)$$

in calculating the real part (hypersingular portion) and the imaginary part (weakly singular portion) of the hypersingular integral (65) in terms of the CPU time is presented. For the sake of a fair comparison, we selected two of the most proven methods available in the literature, i.e., the singularity subtraction method presented by Ylä-Oijala and Taskinen in [19] and the direct evaluation method applied over the static integral, again in a singularity subtraction fashion, presented by Gray *et al.* [26]. Without entering into much detail, the solution from the aforementioned singularity subtraction method is obtained with the subtraction of the first two terms of the Taylor expansion of the free-space Green's function G

$$\nabla G = \nabla\left(G - \frac{1}{R} + \frac{k^2}{2}R\right) + \nabla\frac{1}{R} - \frac{k^2}{2}\nabla R. \qquad (68)$$

The integrals related to the last two terms of the expression above can be computed semi-analytically, where the remaining numerical integrals apply only to smooth functions. The first term has a continuous derivative and, therefore, it can be integrated numerically as well. The choice of removing two terms is somehow optimum as there is not a real improvement after removing more terms. The number of integration points for the singularity subtraction method is fixed for the inner integral and a Gaussian quadrature tailored for triangles [28] is used for the outer integral.

Moreover, the reference solution has been obtained by means of the proposed method in combination with the symbolic software *Maple*, using high precision arithmetic (300 digits) in all the computations together with a high number of integration points until it converges smoothly up to any desired accuracy. The exact value up to 32 significant digits equals

$$I = 3.4928883683897266018383577695620 \cdot 10^{-3}$$
$$- j2.2540732129690316163209769145458 \cdot 10^{-5}. \qquad (69)$$

According to the results, as depicted in Fig. 7, the proposed method converges up to machine precision, even for the hypersingular portion, much faster than the rest. To the best of our knowledge, there is no method readily available in the literature that could provide better accuracy in reasonable computational times. The behavior of the proposed method clearly reveals one of its key features, i.e., the remaining integrands after analytical integrations and reordering are sufficiently smooth functions. Hence, simple interpolatory quadratures, like the standard Gauss-Legendre, are sufficient even for highly accurate results.

This is not the case, though, for the other competing methods, where the remaining integrands after the cancellation or the subtraction of the singularity are non sufficiently smooth functions of the outer (observation) triangle's arguments. The accurate integration of such functions calls for sophisticated 2-D cubatures, like the recently developed double-exponential based generalized Cartesian product rules [29], still with considerable computational overhead. This problem would therefore arise in any of the traditional singularity cancellation or singularity subtraction methods mentioned in the introduction, considering that all of them deal separately with inner and outer integrals.

As for the imaginary part, it seems that the singularity subtraction method stagnates at a relative error of 10^{-7}. A fair explanation of this behavior is based on the fact that the fixed number of integration points used for the inner integral is not sufficient for high precision and it should be increased, deteriorating even more its overall efficiency.

Although the example presented above stands as a representative case in the vast majority of the state-of-the-art triangular meshing schemes, two additional extreme cases have been selected in order to highlight the robustness of the proposed method against deformed triangles with bad aspect ratio or
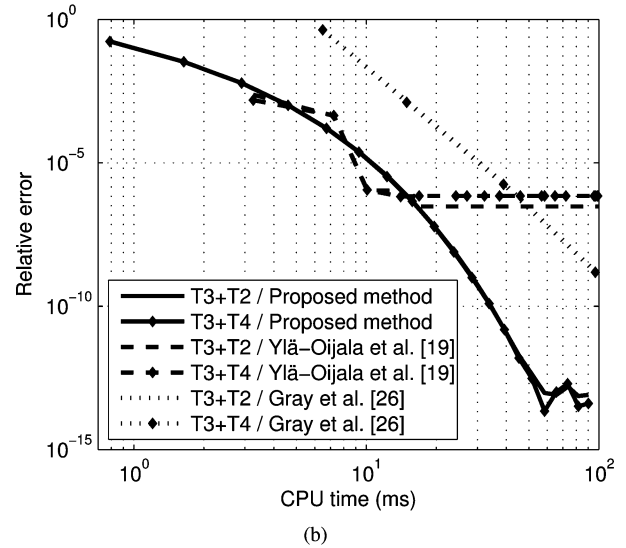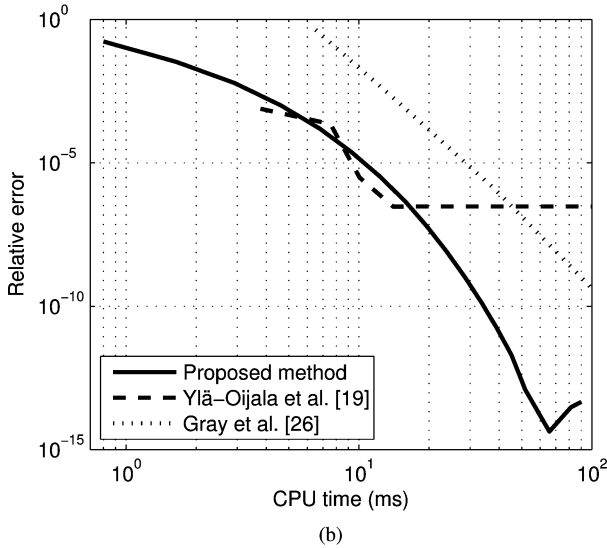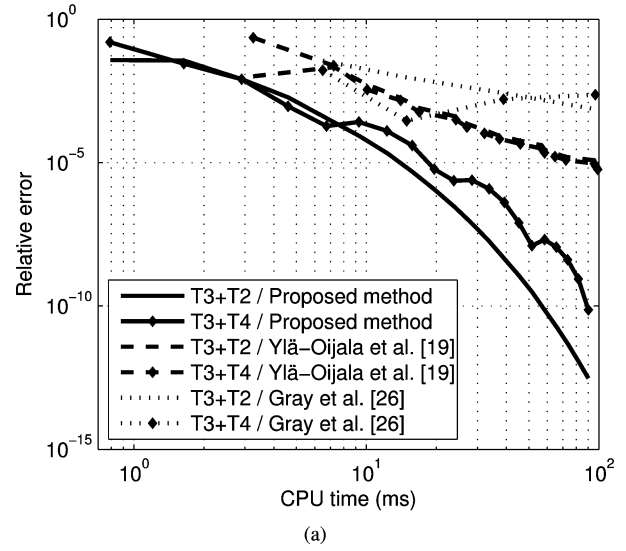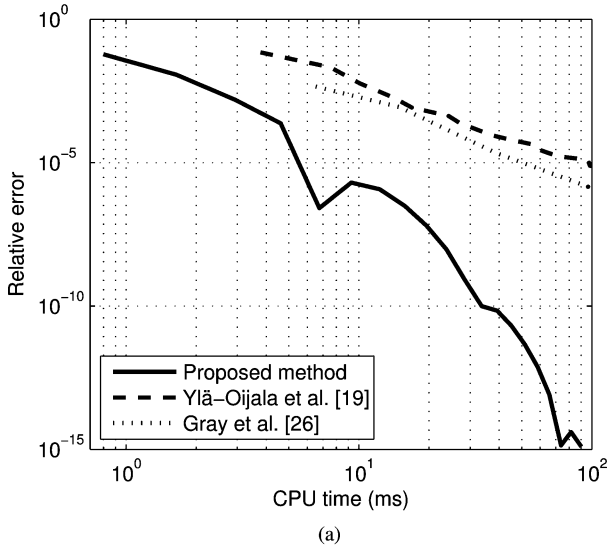
Fig. 7. Comparison of the relative error as a function of the CPU time for the triangles T1 and T2. (a) Real part. (b) Imaginary part.

Fig. 8. Comparison of the relative error as a function of the CPU time for the distorted triangles. (a) Real part. (b) Imaginary part.

quality. One commonly used quality measure for such "distorted" triangles is the ratio between the radius of the largest inscribed circle (times two) and the smallest circumscribed circle

$$q = 2\frac{r_{\text{in}}}{r_{\text{out}}}. \tag{70}$$

According to [30], a triangle with quality factor q lower than 0.7 or a minimum angle lower than 30 degrees is unacceptable in a mesh, and there are techniques to convert these bad meshes into others, fulfilling those requirements [31]–[33]. Therefore, we have selected two triangles T3: $\{\mathbf{r}_1, \mathbf{r}_2, \mathbf{r}_5\}$ and T4: $\{\mathbf{r}_1, \mathbf{r}_2, \mathbf{r}_6\}$ which are below this limit (quality factor of 0.46 and minimum angle of 30 degrees), i.e.

$$\mathbf{r}_5 = [-0.05\lambda, 0.087\lambda, 0]; \quad \mathbf{r}_6 = [-0.05\lambda, 0, 0.087\lambda]. \tag{71}$$

The results for the combinations of triangles $T3+T2$ and $T3+T4$ are depicted in Fig. 8. The reference solutions have

been obtained in the same way as the previous case and they equal, respectively

$$I = 3.141995573252506250493104186 2416 \cdot 10^{-3}$$
$$- j1.960023948755681788930912916 6796 \cdot 10^{-5} \tag{72}$$

$$I = 3.522621701944672762813976584 1737 \cdot 10^{-3}$$
$$- j1.713515137412005944036803270 2308 \cdot 10^{-5}. \tag{73}$$

Although convergence slightly deteriorates for the real part, the proposed method is still able to practically reach machine precision in less than 0.1 s and the same conclusions as in the previous, more representative case can be drawn.

Evidently, the regularization of the hypersingular kernel together with the reduction of the dimensionality of the original integral from 4-D to 2-D via the direct evaluation method has resulted in formulas which provide *numerically exact* results (more than 13 significant digits for the relative error) with
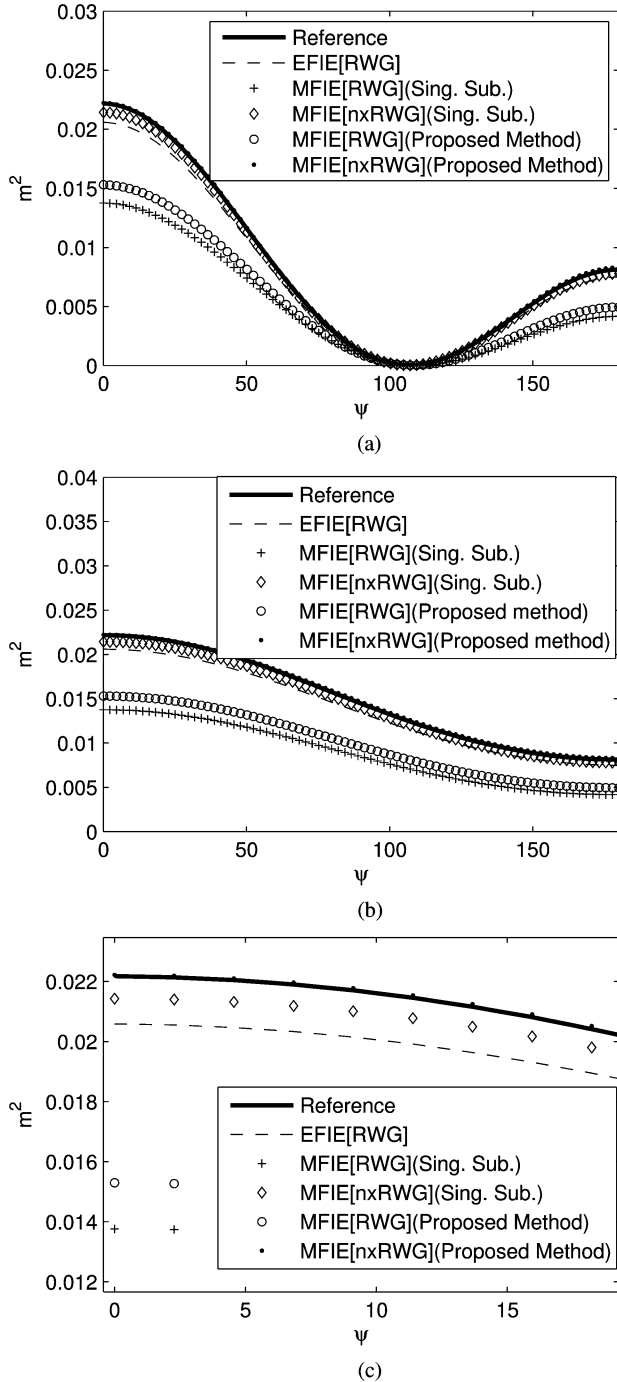
Fig. 9. Bistatic radar cross section (RCS) of a 0.25 λ regular tetrahedron. (a) E-plane. (b) H-plane. (c) E-plane zoomed in.

TABLE II
FUNCTIONS $V_i(B, \Delta_1, \Delta_2)$

$$V_i(B, \Delta_1, \Delta_2) = \int_0^H M_i\left(\eta, \frac{\Delta_1}{1+H}(1+\eta), B\right) d\eta$$

$$+ \int_H^1 M_i(\eta, \Delta_2(1-\eta), B)\, d\eta, \quad H = 1 - \frac{\Delta_1}{\Delta_2}$$

$$a = jkB; \quad H = 1 - \frac{\Delta_1}{\Delta_2}; \quad \Delta_3 = \frac{\Delta_1}{1+H}$$

$$V_1 = 1; \quad V_6 = \frac{1}{2}; \quad V_7 = \frac{1}{3}$$

$T_1^1 = \frac{e^{-a\Delta_3} - e^{-a\Delta_1}}{a\Delta_3}$	$T_1^2 = \frac{1 - e^{-a\Delta_1}}{a\Delta_2}$
$T_2^1 = \frac{T_1^1 - He^{-a\Delta_1}}{a\Delta_3}$	$T_2^2 = \frac{1 - He^{-a\Delta_1} - T_1^2}{a\Delta_2}$
$T_3^1 = \frac{2T_2^1 - H^2 e^{-a\Delta_1}}{a\Delta_3}$	$T_3^2 = \frac{1 - H^2 e^{-a\Delta_1} - 2T_2^2}{a\Delta_2}$
$T_4^1 = \frac{3T_3^1 - H^3 e^{-a\Delta_1}}{a\Delta_3}$	$T_4^2 = \frac{1 - H^3 e^{-a\Delta_1} - 3T_3^2}{a\Delta_2}$
$V_2^1 = T_1^1$	$V_2^2 = T_1^2$
$V_3^1 = \Delta_3(T_1^1 + T_2^1)$	$V_3^2 = \Delta_2(T_1^2 - T_2^2)$
$V_8^1 = T_2^1$	$V_8^2 = T_2^2$
$V_9^1 = T_3^1$	$V_9^2 = T_3^2$
$V_{10}^1 = \Delta_3(T_2^1 + T_3^1)$	$V_{10}^2 = \Delta_2(T_2^2 - T_3^2)$
$V_{11}^1 = \Delta_3(T_3^1 + T_4^1)$	$V_{11}^2 = \Delta_2(T_3^2 - T_4^2)$
$V_{12}^1 = \Delta_3(V_{10}^1 + V_{11}^1)$	$V_{12}^2 = \Delta_2(V_{10}^2 - V_{11}^2)$
$V_4^1 = \Delta_3(V_3^1 + V_{10}^1)$	$V_4^2 = \Delta_2(V_3^2 - V_{10}^2)$
$V_5^1 = \Delta_3(V_4^1 + V_{12}^1)$	$V_5^2 = \Delta_2(V_4^2 - V_{12}^2)$

$$V_i = V_i^1 + V_i^2 \qquad i \in \{2, 3, 4, 5, 8, 9, 10, 11, 12\}$$

TABLE III
FUNCTIONS $U_i(B, \Delta)$

$$U_i(B, \Delta) = V_i(B, \Delta, \Delta) = \int_0^1 M_i(\eta, \Delta(1-\eta), B)\, d\eta$$

$$a = jkB$$

$T_1 = \frac{1 - e^{-a\Delta}}{a\Delta}$	$U_3 = \Delta(T_1 - T_2)$	$U_{11} = \Delta(T_3 - T_4)$
$T_2 = \frac{1 - T_1}{a\Delta}$	$U_6 = \frac{1}{2}$	$U_{12} = \Delta(U_{10} - U_{11})$
$T_3 = \frac{1 - 2T_2}{a\Delta}$	$U_7 = \frac{1}{3}$	$U_4 = \Delta(U_3 - U_{10})$
$T_4 = \frac{1 - 3T_3}{a\Delta}$	$U_8 = T_2$	$U_5 = \Delta(U_4 - U_{12})$
$U_1 = 1$	$U_9 = T_3$	
$U_2 = T_1$	$U_{10} = \Delta(T_2 - T_3)$	

significantly reduced computational effort. In particular, using codes implemented in MATLAB and run in a computer with an Intel Core 2 Quad, 2.83 GHz (no parallelization has been done), Linux 2.6.28 Ubuntu and MATLAB 7.7.0.0.471, the proposed scheme reaches a relative error smaller than 10^{-5} in 10 ms and almost machine precision in about 100 ms.

Finally, a relevant example is presented which shows the importance of leading an accurate integration of the Method of Moments matrix elements. More specifically, an electrically small regular tetrahedron with side 0.25 λ has been chosen and modeled with a very coarse regular mesh of $N = 150$

edges or basis functions, where all the triangles are equilateral. The reference value has been obtained with a very fine mesh ($N = 23436$ edges), accumulating many triangular elements close to the tetrahedron edges and solving with EFIE formulation. The following five simulations have been performed for the coarse mesh: 1) Standard EFIE 2), 3) MFIE with RWG and $\hat{n} \times$ RWG basis functions, respectively, together with standard

singularity subtraction approach, 4), 5) MFIE with RWG and $\hat{\mathbf{n}} \times$ RWG basis functions, respectively, with the edge adjacent interactions computed with the proposed method. Note, that using $\hat{\mathbf{n}} \times$ RWG basis functions imply the same singular integrals [34], [35]. For the singularity subtraction, four integration points per triangle were used. Fig. 9 shows the bi-static RCS for all the cases. Clearly, MFIE with RWG basis functions has the worst performance, although there is a substantial gain when the edge-adjacent integration is done accurately. In this case there is an important error inherent to the formulation itself. However, when using MFIE with $\hat{\mathbf{n}} \times$ RWG basis functions, the performance is even better than with EFIE for the same mesh and an excellent result, without computational overhead, is obtained if the integration is accurately done with the proposed method, as highlighted when zooming in [see Fig. 9(c)]. Moreover, the fast and accurate evaluation of the matrix elements, allows to the proper study of the other (of different nature) well-known problems appearing in MFIE formulations.

V. Conclusion

In this paper, the direct evaluation method is developed for the computation of the hypersingular integrals arising in Galerkin surface integral equation formulations. The key feature of the proposed scheme lies on the appropriate regularization of the singular integrand together with the reduction of the dimensionality of the original integral from 4-D to 2-D. The final formulas presented herein succeed in providing numerical results of unmatched accuracy (close to the machine precision) and efficiency, thus, improving substantially the accuracy of the impedance matrix elements in field integral equation formulations as well as reducing the overall filling time. In addition, we hope that with the detailed analysis and the ready-to-use form of the final formulas, the direct evaluation method will find its place in standard mathematical subroutine libraries widely used in the computational electromagnetics community.

Appendix
Implementation of $N_i^\alpha(B, \theta, \Psi)$ Functions

To compute the $N_i^\alpha(B, \theta, \Psi)$ in an efficient and compact way, we first introduce the following functions:

$$\Delta^a(\theta, \Psi) = \frac{2\sqrt{3}}{\cos(\Psi)(\sin(\theta) + \sqrt{3}\cos(\theta) + \tan(\Psi))}$$

$$\Delta^b(\theta, \Psi) = \frac{\sqrt{3}}{\cos(\Psi)\sin(\theta)}$$

$$\Delta^c(\theta, \Psi) = \frac{\sqrt{3}}{\sin(\Psi)}$$

$$\Delta^d(\theta, \Psi) = \frac{\sqrt{3}}{\cos(\Psi)(\sin(\theta) - \sqrt{3}\cos(\theta))}. \tag{74}$$

The aimed functions can then be calculated in terms of two auxiliary functions $V_i(B, \Delta_1, \Delta_2)$ and $U_i(B, \Delta)$ (actually one, considering $U_i(B, \Delta) = V_i(B, \Delta, \Delta)$) which are defined in Tables II and III, respectively, as

$$N_i^a(B, \theta, \Psi) = V_i(B, \Delta^a(\theta, \Psi), \Delta^c(\theta, \Psi))$$
$$N_i^b(B, \theta, \Psi) = V_i(B, \Delta^b(\theta, \Psi), \Delta^d(\theta, \Psi))$$

$$N_i^c(B, \theta, \Psi) = U_i(B, \Delta^c(\theta, \Psi))$$
$$N_i^d(B, \theta, \Psi) = U_i(B, \Delta^d(\theta, \Psi)). \tag{75}$$

Acknowledgment

References

[1] A. J. Poggio and E. K. Miller, *Integral Equation Solutions of Three Dimensional Scattering Problems*, R. Mittra, Ed. Oxford, U.K.: Permagon, 1973.

[2] J. R. Mosig, R. C. Hall, and F. E. Gardiol, *Numerical Analysis of Microstrip Patch Antennas*, James and Hall, Eds. London, U.K.: IEE-Peter Peregrinus, 1989.

[3] W. C. Chew, J. M. Jin, J. M. Michielssen, and J. M. Song, *Fast and Efficient Algorithms in Computational Electromagnetics*. Boston, MA: Artech House, 2001.

[4] R. F. Harrington, *Field Computation by Moment Methods*. New York, Krieger: Macmillan, 1983.

[5] M. S. Tong and W. C. Chew, "Superhyper singularity treatment for solving 3D electric field integral equations," *Microw. Opt. Tech. Lett.*, vol. 49, no. 6, pp. 1383–1388, Jun. 2007.

[6] M. S. Tong and W. C. Chew, "On the near-interaction elements in integral equation solvers for electromagnetic scattering by three-dimensional thin objects," *IEEE Trans. Antennas Propag.*, vol. 57, no. 8, pp. 2500–2506, Aug. 2009.

[7] S. M. Rao, D. R. Wilton, and A. W. Glisson, "Electromagnetic scattering by surfaces of arbitrary shape," *IEEE Trans. Antennas Propag.*, vol. 30, no. 5, pp. 409–418, May 1982.

[8] A. G. Polimeridis and T. V. Yioultsis, "On the direct evaluation of weakly singular integrals in Galerkin mixed potential integral equation formulations," *IEEE Trans. Antennas Propag.*, vol. 56, no. 9, pp. 3011–3019, Sep. 2008.

[9] C. Schwab and W. L. Wendland, "On numerical cubatures of singular surface integrals in boundary element methods," *Numer. Math.*, vol. 62, pp. 343–369, 1992.

[10] S. Chakraborty and V. Jandhyala, "Evaluation of Green's function integrals in conducting media," *IEEE Trans. Antennas Propag.*, vol. 52, no. 12, pp. 3357–3363, Dec. 2004.

[11] H. X. Zhou, W. Hong, and G. Hua, "An accurate approach for the calculation of MoM matrix elements," *IEEE Trans. Antennas Propag.*, vol. 54, no. 4, pp. 1185–1191, Apr. 2006.

[12] P. W. Fink, D. R. Wilton, and M. A. Khayat, "Simple and efficient numerical evaluation of near-hypersingular integrals," *IEEE Antennas Wireless Propag. Lett.*, vol. 7, pp. 469–472, 2008.

[13] Ismatullah and T. F. Eibert, "Adaptive singularity cancellation for efficient treatment of near-singular and near-hypersingular integrals in surface integral equation formulations," *IEEE Trans. Antennas Propag.*, vol. 56, no. 1, pp. 274–278, Jan. 2008.

[14] S. Caorsi, D. Moreno, and F. Sidoti, "Theoretical and numerical treatment of surface integrals involving the free-space Green's function," *IEEE Trans. Antennas Propag.*, vol. 41, no. 9, pp. 1296–1301, Sep. 1993.

[15] R. D. Graglia, "On the numerical integration of the linear shape functions times the 3-D Green's function or its gradient on a plane triangle," *IEEE Trans. Antennas Propag.*, vol. 41, no. 10, pp. 1448–1455, Oct. 1993.

[16] T. F. Eibert and V. Hansen, "On the calculation of potential integrals for linear source distributions on triangular domains," *IEEE Trans. Antennas Propag.*, vol. 43, no. 12, pp. 1499–1502, Dec. 1995.

[17] R. E. Hodges and Y. Rahmat-Samii, "The evaluation of MFIE integrals with the use of vector triangle basis functions," *Microw. Opt. Tech. Lett.*, vol. 14, no. 1, pp. 9–14, Jan. 1997.

[18] A. Herschlein, J. v. Hagen, and W. Wiesbeck, "Methods for the evaluation of regular weakly singular and strongly singular surface reaction integrals arising in method of moments," *ACES J.*, vol. 17, no. 1, pp. 63–73, Mar. 2002.

[19] P. Ylä-Oijala and M. Taskinen, "Calculation of CFIE impedance matrix elements with RWG and $\hat{n} \times$ RWG functions," *IEEE Trans. Antennas Propag.*, vol. 51, no. 8, pp. 1837–1846, Aug. 2003.

[20] S. Järvenpää, M. Taskinen, and P. Ylä-Oijala, "Singularity extraction technique for integral equation methods with higher order basis functions on plane triangles and tetrahedra," *Int. J. Numer. Methods Eng.*, vol. 58, pp. 1149–1165, Aug. 2003.

[21] A. Tzoulis and T. F. Eibert, "Review of singular potential integrals for method of moments solutions of surface integral equations," *Adv. Radio Sci.*, vol. 2, pp. 93–99, 2004.

[22] L. Gürel and Ö. Ergül, "Singularity of the magnetic-field integral equation and its extraction," *IEEE Antennas Wireless Propag. Lett.*, vol. 4, pp. 229–232, 2005.

[23] I. Hänninen, M. Taskinen, and J. Sarvas, "Singularity subtraction integral formulae for surface integral equations with RWG, rooftop and hybrid basis functions," *Prog. Electromagn. Res. PIER*, vol. 63, pp. 243–278, 2006.

[24] S. Järvenpää, M. Taskinen, and P. Ylä-Oijala, "Singularity subtraction technique for high-order polynomial vector basis functions on planar triangles," *IEEE Trans. Antennas Propag.*, vol. 54, no. 1, pp. 42–49, Jan. 2006.

[25] L. J. Gray, J. M. Glaeser, and T. Kaplan, "Direct evaluation of hypersingular Galerkin surface integrals," *SIAM J. Sci. Comput.*, vol. 25, no. 5, pp. 1534–1556, 2004.

[26] L. J. Gray, A. Salvadori, A. V. Phan, and A. Mantic, "Direct evaluation of hypersingular Galerkin surface integrals. II," *Electron. J. Boundary Elements*, vol. 4, no. 3, pp. 105–130, 2006.

[27] A. G. Polimeridis and J. R. Mosig, "Complete semi-analytical treatment of weakly singular integrals on planar triangles via the direct evaluation method," *Int. J. Numer. Methods Eng.*, vol. 83, pp. 1625–1650, 2010.

[28] D. A. Dunavant, "High degree efficient symmetrical Gaussian quadrature rules for the triangle," *Int. J. Numer. Methods Eng.*, vol. 21, pp. 1129–1148, 1985.

[29] A. G. Polimeridis and J. R. Mosig, "Evaluation of weakly singular integrals via generalized Cartesian product rules based on the double exponential formula," *IEEE Trans. Antennas Propag.*, vol. 58, no. 6, pp. 1980–1988, Jun. 2010.

[30] P. Persson and G. Strang, "A simple mesh generator in MATLAB," *SIAM Rev.*, vol. 46, pp. 329–345, 2004.

[31] J. R. Shewchuk, "Triangle: Engineering a 2D quality mesh generator and Delaunay triangulator," *Appl. Computat. Geometry: Towards Geometric Eng.*, vol. 1148, pp. 203–222, 1996.

[32] J. R. Shewchuk, "Delaunay refinement algorithms for triangular mesh generation," *Computat. Geometry: Theory and Appl.*, vol. 22, pp. 21–74, 2002.

[33] P. A. Foteinos, A. N. Chernikov, and N. P. Chrisochoides, "Fully generalized two-dimensional constrained Delaunay mesh refinement," *SIAM J. Sci. Comput.*, vol. 32, pp. 2659–2686, 2010.

[34] E. Ubeda and J. M. Rius, "MFIE MOM-formulation with curl-conforming basis functions and accurate kernel-integration in the analysis of perfectly conducting sharp-edged objects," *Microw. Opt. Technol. Lett.*, vol. 44, no. 4, 2005.

[35] E. Ubeda and J. M. Rius, "Comments on the use of curl-conforming basis functions for the magnetic-field integral equation," *IEEE Trans. Antennas Propag.*, vol. 56, 2008.

Athanasios G. Polimeridis was born in Thessaloniki, Hellas, in 1980. He received the Diploma degree in electrical engineering and the Ph.D. degree from the Department of Electrical and Computer Engineering, Aristotle University of Thessaloniki (AUTH), Thessaloniki, in 2003 and 2008, respectively.

Since October 2008, he has been a Postdoctoral Research Fellow with the Laboratory of Electromagnetics and Acoustics, Ecole Polytechnique Fédérale de Lausanne (EPFL), Lausanne, Switzerland. His research interests include computational electromagnetics, with emphasis on the development and implementation of integral-equation based algorithms.

José M. Tamayo was born in Barcelona, Spain, on October 23, 1982. He received the degree in mathematics and the degree in telecommunications engineering from the Universitat Politècnica de Catalunya (UPC), Barcelona, both in 2006.

In 2004, he joined the Telecommunications Department, Universitat Politècnica de Catalunya (UPC), Barcelona, where he is pursuing the Ph.D. degree in signal and communication theory. His current research interests include accelerated numerical methods for solving electromagnetic problems.

Juan M. Rius (SM'01) received the "Ingeniero de Telecomunicación" degree in 1987 and the "Doctor Ingeniero" degree in 1991, both from the Universitat Politècnica de Catalunya (UPC), Barcelona, Spain.

In 1985, he joined the Electromagnetic and Photonic Engineering Group, Department of Signal Theory and Telecommunications (TSC), UPC, where he currently holds a position of "Catedrático" (equivalent to Full Professor). From 1985 to 1988, he developed a new inverse scattering algorithm for microwave tomography in cylindrical geometry systems. Since 1989, he has been engaged in the research for new and efficient methods for numerical computation of electromagnetic scattering and radiation. He is the developer of the graphical electromagnetic computation (GRECO) approach for high-frequency RCS computation, the integral equation formulation of the measured equation of invariance (IE-MEI), and the multilevel matrix decomposition algorithm (MLMDA) in 3-D. Current interests are the numerical simulation of electrically large antennas and scatterers. He has held positions of Visiting Professor with the Ecole Polytechnique Fédérale de Lausanne (EPFL), Lausanne, Switzerland, from May 1, 1996 to October 31, 1996; Visiting Fellow with City University of Hong Kong from January 3, 1997 to February 4, 1997; "CLUSTER chair" with EPFL from December 1, 1997 to January 31, 1998; and Visiting Professor with EPFL from April 1, 2001 to June 30, 2001. He has more than 45 papers published or accepted in refereed international journals (24 in IEEE TRANSACTIONS) and more than 100 in international conference proceedings.

Juan R. Mosig (S'76–M'87–SM'94–F'99) was born in Cádiz, Spain. He received the electrical engineer degree from the Universidad Politécnica de Madrid, Madrid, Spain, in 1973, and the Ph.D. degree from the Ecole Polytechnique Fédérale de Lausanne (EPFL), Lausanne, Switzerland, in 1983.

In 1976, he joined the Laboratory of Electromagnetics and Acoustics, EPFL. Since 1991, he has been a Professor with EPFL, and since 2000, he has been the Head of the Laboratory of Electromagnetics and Acoustics (LEMA), EPFL. In 1984, he was a Visiting Research Associate with the Rochester Institute of Technology, Rochester, NY, and Syracuse University, Syracuse, NY. He has also held scientific appointments with the University of Rennes, Rennes, France, the University of Nice, Nice, France, the Technical University of Denmark, Lyngby, Denmark, and the University of Colorado at Boulder. He is currently the Chairman of the EPFL Space Center and is responsible for many Swiss research projects for the European Space Agency (ESA). He has authored five book chapters on microstrip antennas and circuits and over 100 reviewed papers. His research interests include EM theory, numerical methods, and planar antennas.

Dr. Mosig has been a member of the Swiss Federal Commission for Space Applications. He is currently a member of the Board of the Applied Computational Electromagnetics Society (ACES), the chairman of the European COST Project on Antennas ASSIST (2007–2011), and a founding member and acting chair of the European Association and the European Conference on Antennas and Propagation (EurAAP and EuCAP).